On the mechanism of microcrack formation in nanocrystalline Fe–Ni electrodeposits

F. CZERWINSKI
Department of Metallurgical Engineering, McGill University, Montreal, H3A 2A7 Canada
Z. KEDZIERSKI
Department of Metallurgy, University of Mining and Metallurgy, Cracow, 30-059 Poland

The microstructure and internal stress of nanocrystalline Fe–13% Ni alloys electrodeposited onto a steel substrate were examined. A deposit growth was accompanied by the formation of microcracks and a reduction in stress level; during an increase in deposit thickness from 0.1 to 50 μm, the internal stress decreased from 1450 to 90 MPa. An explanation of crack formation was proposed on the basis of Griffith's theory of fracture. A critical deposit thickness prior to crack propagation, predicted from the mechanism proposed, was in good agreement with the values obtained from *in-situ* measurements of stress evolution and from direct microscopy observations. The results showed that the thickness of deposits exerted crucial influence on their fracture resistance.

1. Introduction

Electrodeposition is an effective way to manufacture nanocrystalline materials. It has been successfully used to obtain nanocrystalline Ni–Fe alloys in a wide range of concentrations of both elements. It is known that the nanocrystalline structure leads to enhancement of the magnetic properties of alloys rich in Ni [1]. Conversely, the nanocrystalline structure gives the alloys rich in Fe a high wear resistance exceeding the level achieved for tempered steel [2].

A major drawback in the electrodeposition of nanocrystalline materials is the generation of high internal stress (macrostress). This factor is of special importance since, according to the coalescence theory of stress origin, there is a correlation between internal stress and grain size [3]. Therefore, in many cases, the various components are added to the electrolyte to reduce the stress level [4]. The evident result of stress generation is the formation of microcracks. It is obvious that, in many applications, the microcracks limit the exploitation of deposits; they may cause localized corrosion or a decrease in fatigue life, or in extreme cases they may lead to deposit spallation from the substrate [4]. A knowledge of the magnitude of the internal stress generated and the mechanism of deposit cracking are therefore important to the design of the deposition parameters and to the control of the mechanical properties of electrolytic metals and alloys.

In this study, we present an analysis of microcrack formation in Fe–13% Ni nanocrystalline alloys deposited onto steel substrate. On the basis of *in-situ* stress measurement and microstructural characterization an explanation of the deposit fracture is proposed.

2. Experimental procedures

The electrolyte used for alloy deposition was composed of nickel chloride and ferrous chloride with concentrations of 200 $g l^{-1}$ and 300 $g l^{-1}$, respectively. The pH was kept constant at a level of 1.5 by adding hydrochloric acid. Fe–Ni alloys were deposited onto a steel substrate at an electrolyte temperature of 25 °C and at a current density of 150 mA cm^{-2}. The substrate was prepared by mechanical polishing using SiC paper of up to 800 grit, followed by chemical polishing in 10% hydrochloric acid. The microstructural characterization was performed on planar and cross-sectional polished sections using optical microscopy, and on carbon replicas using transmission electron microscopy (TEM). To increase the image contrast, the replicas were shadowed with thin platinum film.

The internal stress was measured *in-situ* using a device based on the flexible-beam technique [5, 6]. The value of an average stress σ generated in the deposit was calculated according to the formula [7]

$$\sigma = \frac{Ez(t_s^2 + t_s t_1)}{3t_1 L^2} \quad (1)$$

where z is a displacement of the coated part of the substrate with a length of L; t_s and t_1 are thicknesses of the substrate and deposit, respectively, and E is Young's modulus for the carbon steel substrate. Assuming a constant deposition rate, the deposit thickness was calculated from a metallographic cross-section after completion of measurement. The experimental details of stress measurement have been published elsewhere [8].

0022–2461

3. Results

3.1. Microstructure of electrodeposits

Fe–Ni electrodeposits obtained under the conditions of this experiment contained approximately 13% Ni and were represented by a solid solution of Ni in α-Fe. An average microhardness measured using a Vickers indenter under a 100 g load on polished cross-sections at varying distances from the substrate–deposit interface was 647 HV with a standard deviation of 9 HV. No evident changes in microhardness versus deposit thickness were detected.

The growth surface of the deposit was flat with a mirror-like appearance. Observations using optical microscopy revealed the presence of microcracks (Fig. 1a). In a planar view, the microcracks exhibited a characteristic pattern. A closer examination revealed that this pattern is formed by the superimposed networks of microcracks. In Fig. 1a, at least three networks are seen, each with a different intensity, presumably caused by the differences in crack width. The parts of those networks are labelled 1, 2, and 3 in Fig. 1a, in the direction of decreasing intensity. A cross-sectional observation showed that the microcracks were oriented perpendicular to the substrate–deposit interface, and to a first approximation they were evenly distributed over the deposit thickness (Fig. 1b). At the magnification used with the optical microscope, which was not high enough to distinguish clearly between the ferrite and cementite in pearlite, it was impossible to establish the correlation between the phase component of the substrate and the density of microcracks in the adjacent part of the deposit. On the assumption, however, that the pearlite is one structural component, the microcrack density over both the ferrite and the pearlite areas was the same.

Because the deposits were very brittle, an attempt to prepare thin foils for TEM was unsuccessful. TEM observation of growth morphology of the deposit using the carbon replica technique revealed nano-sized growth features. In Fig. 2a, some of them are indicated by arrows. The grain size estimated from those features is in the range 20–50 nm. This is in general agreement with the conclusion which can be obtained from observation of the carbon replica of an etched cross-section (Fig. 2b). Moreover, the cross-sectional view revealed the lamellar substructure of the deposit. The individual layers with thicknesses of 100–400 nm were oriented perpendicular to the growth direction and exhibited features which were similar in shape and size to those observed in the planar view (Fig. 2a). The formation of such a lamellar structure is explained by some workers to be the result of periodic changes in the pH of the electrolyte and occlusion of hydroxides

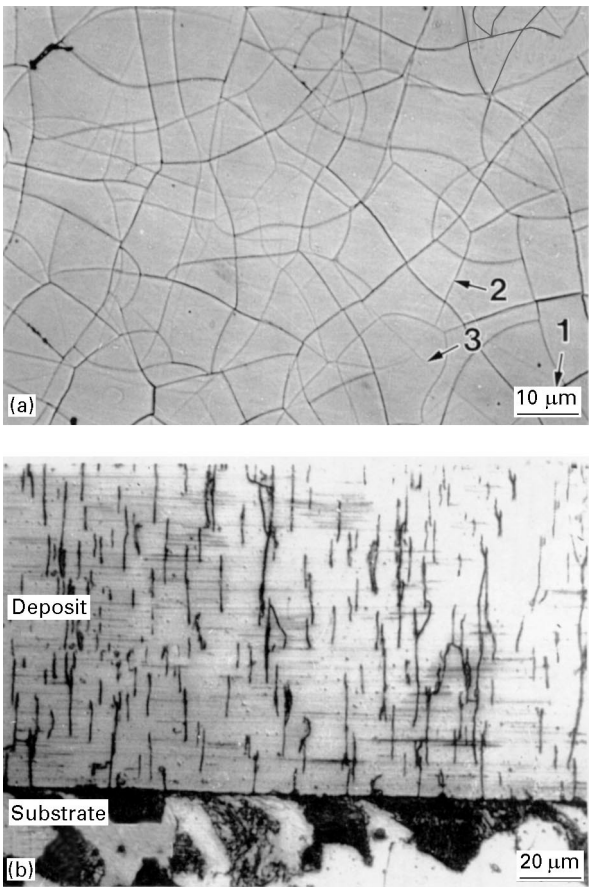

Figure 1 Optical micrographs of Fe–Ni deposit: (a) planar view of the growth surface showing the network of microcracks (surface without etching); (b) cross-sectional view after etching with 3% nitric acid in ethanol, showing the microcracks oriented prependicular to the substrate.

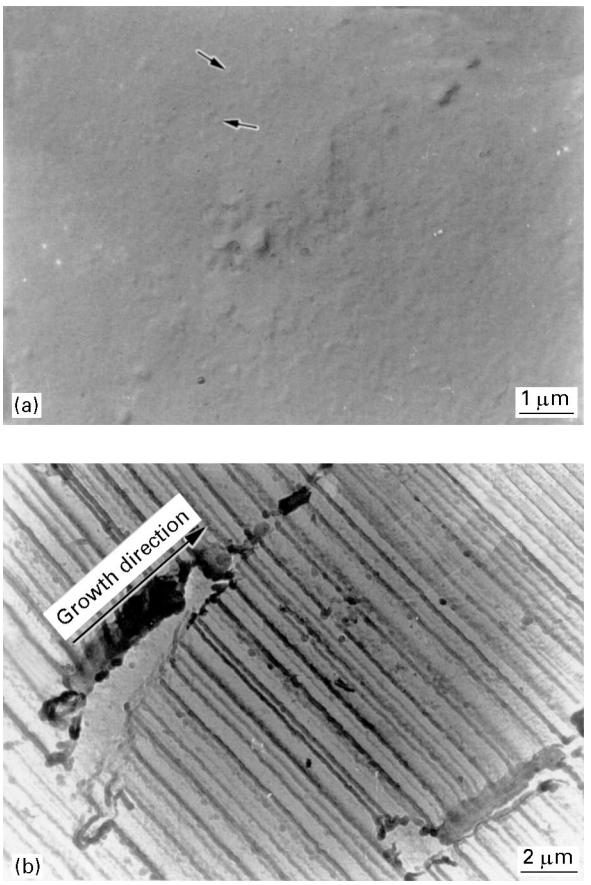

Figure 2 TEM images of Fe–Ni films obtained using carbon replicas: (a) planar view of growth surface in the region between microcracks showing the individual crystallites with a size between 20 and 50 nm; (b) cross-sectional image showing the morphology of individual microcracks and the microstructure of lamellar deposit (before preparation of replica, the deposit was etched with 3% nitric acid in ethanol to reveal the microstructural features).

on the growth surface [2, 9], or periodic incorporation of trace amounts of metallic impurities [10].

3.2. Stress generation during growth of electrodeposits

The deflection of the flexible beam of steel with a length $L = 57$–59 mm and a thickness $t_s = 0.345$–0.353 mm during one-side deposition of Fe–Ni alloy is shown in Fig. 3. The direction of bending towards the coated side supports the origin of tensile stress in the deposit. For the conditions of this study, the total beam deflection z, measured *in situ* during deposit growth, did not exceed 2 mm. To diminish the influence of small differences in size of individual beams, the modified deflection is plotted in Fig. 4 as $z(t_s/L)^2$.

The measured values of beam deflections were then used to calculate the average stress according to Equation 1. As Young's modulus for the steel substrate, a value of 2×10^5 MPa has been taken [11]. The average stress plotted as a function of deposit thickness is shown in Fig. 5. There it is seen that, in general, the continuous reduction in stress from 1450 to about 90 MPa took place as the deposit grew from 0.1 to 50 μm. However, a closer analysis of the initial periods of deposit growth revealed that two stages on the stress curve can be distinguished (Fig. 5, inset). To separate these stages, the experimental points were described by two power relationships using the least-squares method. The first, which is expressed as

$$\sigma\,(\mathrm{MPa}) = 1173.4 t_l^{-0.08}\ (\mu\mathrm{m}) \qquad (2)$$

and is shown as curve 1 in the inset of Fig. 5, covers the deposit thicknesses between 0.1 and 1.03 μm. Curve 2 is described by the formula

$$\sigma\ (\mathrm{MPa}) = 1190.9 t_l^{-0.68}\ (\mu\mathrm{m}) \qquad (3)$$

and covers the deposit thicknesses in the range 1.03–50 μm. To estimate the goodness of the fit of the curves to the experimental points, the standard deviation of experimental values of σ from the corresponding values of σ obtained from Equations 2 and 3 was used. The values of 59.5 and 69.8 MPa obtained for standard deviations of curves given by Equations 2 and 3, respectively, show that the fitted curves described the experimental data well.

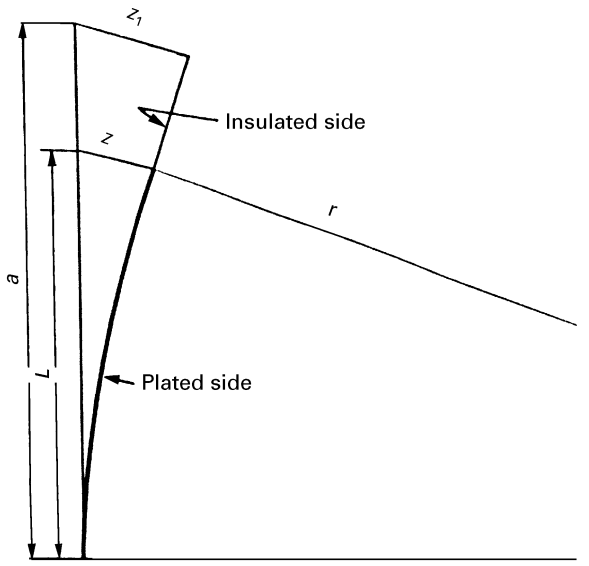

Figure 3 Schematic diagram of the flexible beam of carbon steel used for stress measurement (dimensions: total beam length, $a \sim 80$ mm; length of coated part, $L = 57$–59 mm; beam thickness, $t_s = 0.345$–0.353 mm; beam width, 10 mm; total deflection, $z < 2$ mm).

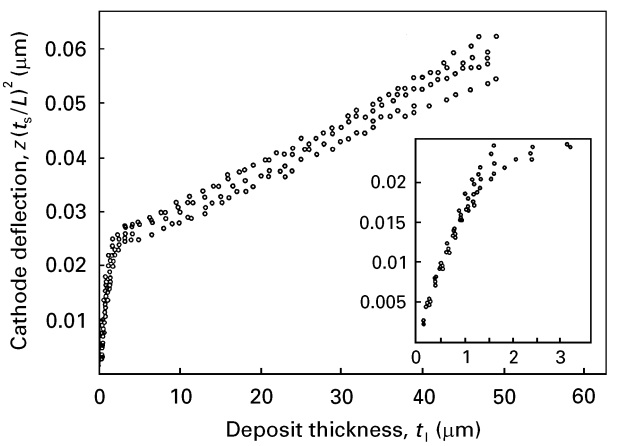

Figure 4 The beam deflection measured *in-situ* during deposition of Fe–Ni alloy at a temperature of 25 °C and a current density of 150 mA cm^{-2}.

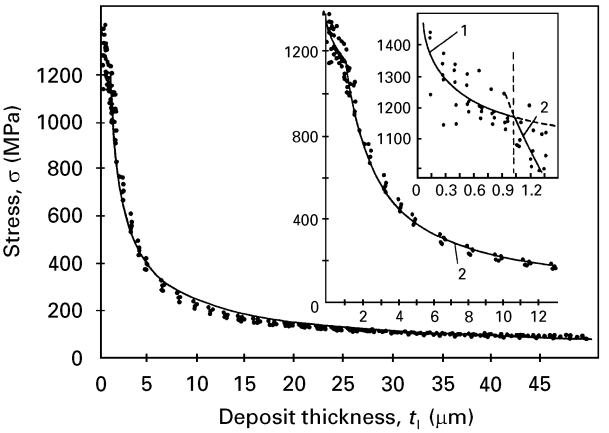

Figure 5 The stress measured *in-situ* during the growth of Fe–Ni alloy at a current density, I_d, of 150 mA cm^{-2} and an electrolyte temperature of 25 °C. Curve 1 is described by the equation $\sigma\ (\mathrm{MPa}) = 1173.4 t_l^{-0.08}$ (μm); curve 2 is described by $\sigma\ (\mathrm{MPa}) = 1190.9 t_l^{-0.68}$ (μm).

3.3. Analysis of deposit fracture

Microscopy observations of the growth surfaces of Fe–Ni thin films formed during the initial stages of electrodeposition confirmed that they were crack free. Only the deposits thicker than approximately 1 ± 0.2 μm contained microcracks. This corresponds to the deposit thickness at which the rapid stress relief was detected (Fig. 5).

In order to explain the microcrack formation, Griffith's theory of brittle fracture was applied [12]. To adjust this theory to brittle deposits with a high level of hardness, the dependence between the fracture stress σ and the critical crack length c was expressed

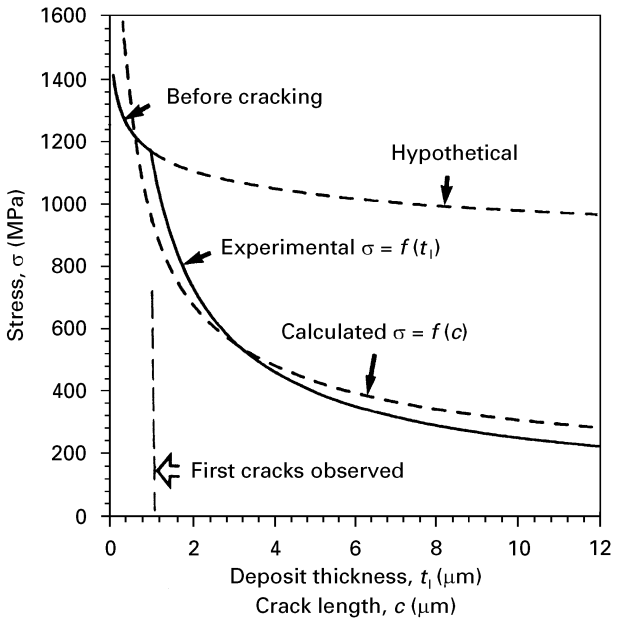

Figure 6 The plots of experimental values of internal stress versus deposit thickness $\sigma = f(t_1)$ and the calculated fracture stress versus crack length $\sigma = f(c)$. The thickness at which the deposit fracture was observed microscopically is indicated.

by the modified Griffith's formula

$$\sigma = \left(\frac{E\gamma_{\text{eff}}}{\pi c}\right)^{0.5} \tag{4}$$

where E is Young's modulus and γ_{eff} is the effective surface energy. The modification of the original Griffith's formula [12], applicable to perfectly brittle material, is expressed by a change in the surface energy component γ_s to γ_{eff}, which includes a plastic deformation of the material [13]. Since the values of E and γ_{eff} for Fe–13% Ni alloy with such a specific microstructure were not available, in further calculations they were substituted by the literature data for ferrite. Thus on the assumption that $E = 2.1 \times 10^5$ MPa [11] and $\gamma_{\text{eff}} = 14\ \text{J m}^{-2}$ [13], Equation 4 can be written as

$$\sigma\ (\text{MPa}) = 967.4c^{-0.50}\ (\mu\text{m}) \tag{5}$$

Equation 5 is graphically shown in Fig. 6. In this figure, the stress measured in the deposit is also presented; the continuous part of the curve $\sigma = f(t_1)$ describes the stress in the deposit before cracking (0.1–1.03 μm), and after crack formation (greater than 1.03 μm). According to the experimental curve $\sigma = f(t_1)$, the deposit cracking took place at a stress level of 1170 MPa and at a deposit thickness of 1.03 μm. For the same stress of 1170 MPa, the curve $\sigma = f(c)$ gives the value of 0.68 μm for critical crack length. At the bottom of Fig. 6, the deposit thickness close to 1 ± 0.2 μm is marked, which is the point at which the first microcracks were observed microscopically.

4. Discussion

Both the observations of this study and the literature data [14] indicate that cracking takes place after the electrodeposit reaches a certain critical thickness. For Fe–Ni alloys manufactured at the conditions of this experiment the critical thickness was a 1 ± 0.2 μm, as estimated microscopically. This value is in good agreement with the thickness at which rapid relief of internal stress took place, as seen on both plots: the flexible beam deflection (Fig. 4) and the stress evolution during deposit growth (Fig. 5). It is interesting to note that, despite the great simplification of the fracture mechanism achieved by applying Equations 4 and 5, the plots of measured stress $\sigma = f(t_1)$ and calculated fracture stress $\sigma = f(c)$ are located in coordinate systems close to each other. Also, the value of critical thickness estimated from the fracture stress, i.e., 0.68 μm, is of the same order of magnitude as that evaluated from the internal stress plot and from direct observations.

According to the earlier explanations, the deposit fracture was caused by a gradual increase in stress during deposit growth. When the stress exceeded the fracture strength of the deposit, the cracks propagated. However, literature data are divided on the issue of the existence of stress maximum at thicknesses compared with the critical thickness [15, 16]. Furthermore, our measurements did not reveal the maximum on the stress curve within the thickness range 0.1–50 μm. Thus, the question arises: at what deposit thickness should the stress maximum during electrodeposition be expected?

A precise measurement showed that the stress maximum is almost entirely caused by the extrinsic stress component which is affected by the substrate and should be expected in the vicinity of the substrate–deposit interface before the formation of misfit dislocations. For a particular case of electrodeposition of Ni on Cu, a stress maximum close to 2000 MPa was located at a thickness well below 20 nm [17]. The intrinsic stress component is then developed, which is affected by deposition parameters [3, 8]. It should be mentioned at this point that our experimental set-up allowed a starting measurement in the deposits with a minimum thickness of 0.1 μm. Therefore, we must assume that the stress shown in Fig. 5 entirely represents the intrinsic component. A lack of stress maximum at a thickness of 1 μm thus indicates the necessity of other mechanisms of microcrack formation. Such a simple explanation is proposed in this study.

The stress curve in Fig. 5 shows that, despite the high value of stress in deposits with thicknesses below 1 μm, the cracks did not propagate and the deposits grew in a compact form. It is suggested that the reason for such behaviour is the fact that the deposit thickness was smaller than the critical crack length necessary, according to Equations 4 and 5, for crack propagation at the existing stress level. The evolution of stress represented by curve 1 in Fig. 5 is commonly observed in the compact deposits. For coarse-grained and crack-free deposits, the microstructural changes which accompany such stress evolution have been discussed elsewhere [3]. It is possible that, if the deposit had a hypothetically high fracture strength, the fracture would not take place at a thickness of about 1 μm and the stress evolution would be described by the extrapolation of curve 1 beyond a thickness of

1 μm, labelled hypothetical in Fig. 6. The fracture of brittle deposits at a thickness of about 1 μm caused a rapid decrease in stress, as shown by curve 2. Thus, for the deposits in the thin-film range, the thickness is an additional factor affecting the fracture resistance of the deposits.

Although the deposit fracture explained here is related to the internal stress development characteristic for electrocrystallization, the existence of critical film thickness was also observed for the other systems and techniques of deposition [18]. There are also data relating the density of microcracks to the yield stress of the substrate [19, 20]. According to this finding, some nonuniformity in crack density should be seen over the ferrite and pearlite regions. Unfortunately, our micrographs do not show such evidence. The only difference in crack density was caused by changes in deposition parameters, as reported elsewhere [8].

5. Conclusions

Deposition of Fe–13% Ni alloys with a Vickers hardness of 647 HV and a grain size of approximately 20–50 nm, from chloride electrolyte without additions, was accompanied by the generation of high internal stress, leading to fracture of the deposit. The formation of microcracks caused a relief of internal stress; an increase in deposit thickness from 0.1 to 50 μm resulted in a decrease in internal stress from 1450 to 90 MPa.

The deposit fracture was not related to the existence of a maximum on the internal stress–thickness curve. It was shown that the crack propagation occurred when the deposit thickness exceeded the magnitude of critical crack length estimated on the basis of Griffith's theory of fracture. The critical thickness of deposits predicted from the proposed mechanism, i.e., of 0.68 μm, is in good agreement with the value of approximately 1 μm estimated from *in-situ* measurement of internal stress evolution and from the direct microscopy observations of the growth surface.

Acknowledgement

The authors thank Dr. A. Zielinska-Lipiec of The University of Mining and Metallurgy, Cracow, Poland for TEM observations.

References

1. C. CHEUNG, G. PALUMBO and U. ERB, *Scripta Metall. Mater.* **31** (1994) 735.
2. M. P. MIELKOW, "Coating for automotive industry" (Transport, Moscow, 1971).
3. F. CZERWINSKI, *J. Electrochem. Soc.* **143** (1996) 3327.
4. E. RAUB and K. MULLER, "Fundamentals of metals deposition (Elsevier, Amsterdam, 1967).
5. G. G. STONEY, *Proc. R. Soc. A* **32** (1909) 172.
6. S. N. SAHU, J. SCARMINO and F. DECKER, *J. Electrochem. Soc.* **137** (1990) 1150.
7. R. WEIL, *Plating* **12** (1970) 1231.
8. F. CZERWINSKI, *Thin Solid Films* **280** (1996) 199.
9. A. BRENNER, "Electrodeposition of alloys" (Academic Press, New York, 1963).
10. J. M. CHEN and Z. Y. CAI, *Acta Chim. Sinica* **41** (1983) 11.
11. "Metals handbook", Vol. 8 (American Society for Metals, Metals Park, OH, 1985).
12. R. W. HERTZBERG, "Deformation and fracture mechanics of engineering materials" (Wiley, New York, 1976).
13. D. A. CURRY, *Metal Sci.* **8–9** (1980) 319.
14. J. E. KLUSHKIN and A. M. SHIRAEV, *Electrochimia* (*Moscow*) **2** (1996) 155.
15. I. L. NEWELL, *Metal Finish.* **10** (1960) 56.
16. R. KONISHI, *ibid.* **3** (1963) 54.
17. H. FEIGENBAUM and R. WEIL, *J. Electrochem. Soc.* **126** (1979) 2085.
18. M. D. THOULESS, E. OLSSON, and A. GUPTA, *Acta Metal.* **40** (1992) 1287.
19. M. S. HU and A. G. EVANS, *ibid.* **37** (1989) 917.
20. D. C. AGRAWAL and R. RAJ, *ibid.* **37** (1989) 1265.

Received 19 April
and accepted 19 December 1996